

Thermopower generation and thermoelectric cooling in a Kane-Mele normal-insulator-superconductor nano-junction

PRIYADARSHINI KAPRI¹ and SAURABH BASU¹

¹ Indian Institute of Technology Guwahati, Assam-781039, India

PACS 73.40.-c – Electronic transport in interface structures

PACS 74.45.+c – Andreev reflection; NS junction

PACS 74.25.F- – Transport properties

Abstract – We have studied thermoelectric effect of a Kane-Mele normal - insulator - superconductor (KMNIS) junction at ultra-low temperatures using a modified version of the well-known Blonder-Tinkham-Klapwijk (BTK) theory. Since both the (electronic) charge and thermal current due to the carriers are sensitive to the strengths of the spin-orbit coupling (SOC) present in the Kane-Mele model, a tunability of this junction device with regard to its thermoelectric properties can be experimentally achieved by certain techniques that are used to manipulate the values of the spin-orbit couplings. We have computed the Seebeck coefficient, the Figure of Merit, the thermoelectric cooling, the coefficient of performance of the KMNIS junction as a self-cooling device and investigated the role of the Rashba SOC (RSOC) and intrinsic SOC (ISOC) parameters therein. Our results on the thermoelectric cooling indicate practical realizability and usefulness for efficient cooling detectors, sensors, and quantum devices and hence could be crucial to experimental success of the thermoelectric applications of such junction devices. Further we have briefly touched upon the condition that distinguishes transmission through a topological insulator from an ordinary one.

Introduction. – One of the most attracted theoretical attention in the field of condensed matter physics since the several decades has been the study of the graphene [1, 2], a two dimensional single layer of hexagonal lattice of carbon atoms. The conduction and the valance bands in graphene touch each other along the six Dirac points where the quasiparticle excitations show a linear Dirac-like energy dispersion. The unique geometrical structure of graphene has generated tremendous interest in different field of applications, such as, electronics [1–3], optoelectronics [4, 5], and spintronics [6–9]. Further, some other interesting phenomena such as, anomalous quantum Hall effect [10, 11], chiral tunneling [12, 13], Klein paradox [12, 14] have been obtained in graphene. Moreover, the superconducting features can be induced in graphene by possible intercalation with dopant molecules [15] or via proximity effects [16, 17]. Such prospects provide a newer scopes of fabricating devices based on hybrid structures of graphene based superconductors.

Recently, the thermal and thermoelectric properties of graphene structure have gained much attention because of the large Seebeck coefficient and high thermal conductiv-

ity obtained in graphene sheets [18–20]. Previously, due to the experimental limitations in accessing nano-scale devices, the charge and spin dependent thermoelectric properties were often ignored [21, 22]. But recently improved techniques in low temperature measurements devices provides an opportunity of experimental observation of thermoelectric physics. Very recently Zuev et al [19] and Wei et al. [23] have performed theoretical and experimental investigation of the thermoelectric effects of graphene sheets.

Two types of spin-orbit couplings (SOC) are proposed in graphene, the Rashba spin SOC and the intrinsic SOC where it has been predicted by Kane and Mele that the presence of both the spin-orbit term may be the reason behind realizing a new type of topological state which is known as the quantum spin Hall state (QSH) [24]. However owing to the very small strength of the spin gap (typically $\sim 0.01 - 0.05 meV$) [25, 26] in graphene, the QSH state is not achieved in experiments. But there are possible methods available to induce enhanced SOC strengths in graphene, such as via adatoms [27], using proximity effect of a three dimensional topological insulators [28, 29], by functionalization with methyl groups [30] etc. It is ex-

perimentally obtained that in a graphene nano-sheet the RSOC strength can be enhanced up to $17meV$ by proximity effects. Further, it is observed that from gold (Au) intercalation at the graphene-Ni interface [31], the RSOC is enhanced up to approximately $100meV$. A large Rashba splitting about $225 meV$ in epitaxial graphene layers on the surface of Ni [32] and a giant RSOC at the graphene-Ir surface from Pb intercalation have been observed [33]. Moreover the tunability of RSOC strength via an external gate voltage provides an additional impetus in the field of spintronics. It is worth to mention that SOCs are very significant and hence cannot be skipped in the context of charge transport.

In a parallel front, the quantum transport through the junction devices are gaining increased attention in the field of modern research for developing the nano-devices at atomic/molecular level. The junction devices have interesting applications in the fields of thermoelectric, thermometric, solid state cooling etc. In the past a good number of studies on junction has been performed in these fields [34–39] and the junction devices are very useful in wide range of experiments and applications [40–42]. The recent development in the field of thermoelectric physics in small scale junction devices provides a new direction for fabricating self-cooling devices, thermopower devices etc.

Motivated by the above, we have performed an extensive study of the thermoelectric effect of a Kane-Mele normal-insulator-superconductor (KMNIS) nano-junction by employing the modified Blonder-Tinkham-Klapwijk (BTK) theory which describes the low energy transmission characteristics of nano/mesoscopic junctions. Physically the scenario corresponds to adatom decorated graphene NIS junction to account for finite strengths of the spin-orbit couplings. Thus a KMNIS is used interchangeably with adatom decorated graphene NIS junctions. We have computed the spin resolved thermopower, Figure of Merit, thermal current, coefficient of performance and explored how the spin-orbit couplings (induced by adatoms or otherwise) assume roles in shaping up the thermoelectric properties of such a junction.

Theoretical model: BTK approach. – In Fig.(1) the schematic diagram of the junction setup has been shown where the left electrode is a normal ($x \leq 0$) and the right electrode ($x \geq d$) is a superconducting material with the insulating layer is extending from $x = 0$ to $x = d$. V_0 is the potential across the insulating barrier region which can be tuned by an external gate voltage. It is considered that the $x \geq d$ region of the junction system has been produced by proximity effect by an external superconductor.

The effective Hamiltonian for graphene with both the

spin-orbit couplings is given by,

$$\begin{aligned}
 H = & -t_1 \sum_{\langle ij \rangle} a_i^\dagger b_j + i\lambda_I \sum_{\langle\langle ij \rangle\rangle} V_{ij} (a_i^\dagger \sigma_z a_j \\
 & + b_i^\dagger \sigma_z b_j) + i\lambda_R \sum_{\langle ij \rangle} a_i^\dagger (\hat{\sigma} \times \hat{d}_{ij}) \cdot \hat{n} b_j + \lambda_\nu \sum_i a_i^\dagger a_i \\
 & - \lambda_\nu \sum_i b_i^\dagger b_i + h.c.
 \end{aligned}
 \quad (1)$$

The first term denotes the nearest neighbour (NN) hop-

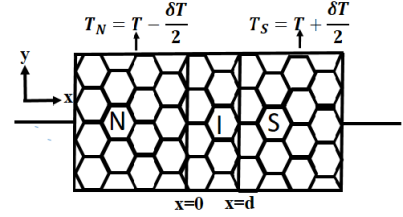


Fig. 1: The KMNIS junction setup.

ping with a hopping strength t_1 , the second term denotes the intrinsic spin-orbit coupling given by the next-nearest neighbours (NNN) hopping with the intrinsic spin-orbit coupling (ISOC) strength λ_I . $\langle\langle ij \rangle\rangle$ represents the summation over NNN, $V_{ij} = +(-)$ if the hopping is clock-(anti clock) wise. The third term indicates Rashba term given by the nearest neighbour (NN) hopping with the Rashba spin-orbit coupling (RSOC) strength λ_R , where \hat{d}_{ij} signifies the unit vector from site i to j , σ denotes Pauli matrices and $\hat{n} = \hat{x}$ is unit vector along the interface normal. An on-site energy term is given by, λ_ν which is different for the two sites within the cell. In particular we have considered " + " energy for A site and " - " energy for B site. Operators a_i^\dagger (b_i^\dagger) denotes the creation and a_i (b_i) denotes the annihilation of an electron at R_i site of the A(B) sublattices. Various details related for the simplification of the Hamiltonian and the BTK formalism applied to the Kane Mele normal-insulator-superconductor nano-junctions appear elsewhere [43].

It is important to note that though in the presence of the RSOC and ISOC, there are opening of gaps in the electronic dispersion (insulating regime) at the valley points (K and K'), the incident particles will still be able to pass through the insulating gap under certain condition. This can be stated as the following. The values of the intrinsic and the Rashba coupling terms should be such that, $\lambda_{I\nu}^2 + \lambda_R^2 < (E_N^F \pm E)^2$ where $\lambda_{I\nu} = \lambda_\nu - \sigma 3\sqrt{3}\lambda_I$, $\lambda_R = 3\lambda_R/2$, E_N^F is the Fermi energy and E is the energy of the carriers. If this condition is violated then there will be no transmission. In a sense this condition may be contemplated to distinguish the topological insulators from that of the ordinary insulators. In this regard, the inset of Fig.(1) of Ref.([48]) may be seen where a diamond shaped region in the λ_R (in units of λ_I) vs λ_ν (scaled by λ_I) is identified as the topological phase where

the transport is possible only via the edge states, while the bulk remains insulating. To compute transport properties using BTK formalism, the above inequality yields a condition for transmission, which, when violated ensures no conductance.

The expression for the charge current through the KNIS junction using BTK theory can be found to have the following form,

$$I_{NS\sigma}(E_F^N, T_N, E_F^S, T_S) = eA_r v_F^N \int \int \tau_\sigma(E, \theta_{N1}) \quad (2)$$

$$[f^N(E_f^N, T^N) - f^S(E_F^S, T_S)]N(E)dE \cos\theta_{N1} d\theta_{N1}$$

where $N(E)$ denotes the density of states, v_F^N is the Fermi velocity, A_r is the area of contact, and f^N, f^S are the Fermi distribution functions for the normal and the superconducting leads respectively. $\tau_\sigma(E, \theta_{N1})$ is the transfer probability where $\tau_\sigma(E, \theta_{N1}) = 1 - |b_\sigma(E, \theta_{N1})|^2 + |a_\sigma(E, \theta_{N1})|^2$, a_σ is amplitude of Andreev reflection, b_σ is amplitude of normal reflection, θ_{N1} is the angle of incidence for electrons. The Fermi energy variation across the junction system is assumed as, $E_F(x) = E_F^N \Theta(-x) + E_F^I \Theta(d-x) + E_F^S \Theta(x-d)$, where E_F^N and E_F^S are the Fermi energies of the normal the superconducting leads. E_F^I is the Fermi energy of the insulating barrier which is defined by, $E_F^I = E_F^N + V_0$, where V_0 is an external gate voltage. As the normal state resistance, R_N is given by, $R_N = \frac{1}{2e^2 N_0 v_F^N A_r}$ (2 comes due to the spin degeneracy, N_0 denotes the density of states at Fermi level), the electrical charge current takes the following form,

$$I_{NS\sigma}(E_F^N, T_N, E_F^S, T_S) = \frac{1}{2eR_N N_0} \int \int \tau_\sigma(E, \theta_{N1}) \quad (3)$$

$$[f^N(E_f^N, T^N) - f^S(E_F^S, T_S)]N(E)dE \cos\theta_{N1} d\theta_{N1}$$

where the energy dependent quantity, $N(E) = \frac{|E_F^N + E|W}{\pi \hbar v_F^N}$ is the number of transverse modes in a graphene sheet of width W [49].

Seebeck coefficient. Here we present the theory to calculate the Seebeck coefficient. A temperature difference between two dissimilar materials produces a voltage difference between the two substances and this phenomenon is known as Seebeck effect. Seebeck coefficient is a measurement of the amount of potential induced in the device for unit temperature difference and defined by, $S = \delta V / \delta T$.

We consider the left and right electrodes serve as independent temperature reservoirs where the left electrode is fixed at temperature, $T^N = T - \delta T / 2$ and the right electrode is fixed at temperature $T^S = T + \delta T / 2$. The population of electrons in the left and the right lead is described by the Fermi-Dirac distribution function, f^N and f^S respectively where $E_F^N = E_F^S$ at zero external bias.

Let us now consider an extra infinitesimal current induced by an additional voltage, δV and the temperature difference, δT across the junction in an open circuit. The current induced by δT and δV are given by,

$(dI)_T = I(E_F^N, T^N, E_F^S = E_F^N, T^S = T^N + \delta T)$ and $(dI)_V = I(E_F^N, T^N, E_F^S = E_F^N + e\delta V, T^S = T^N)$. Suppose that the current cannot flow in an open circuit, thus $(dI)_T$ counter balances $(dI)_V$. It allows us to write,

$$dI = (dI)_T + (dI)_V = 0 \quad (4)$$

where the expression for the $(dI)_T$ and $(dI)_V$ can be obtained from Eqn.(3). Now first order expansion of Fermi-Dirac distribution function in $(dI)_T$ and $(dI)_V$ yields the expression for the spin dependent Seebeck coefficient,

$$S_\sigma = \frac{\delta V}{\delta T} = \frac{\int \int dE d\theta_{N1} \cos\theta_{N1} E (E_F^N + E) \tau_\sigma(E, \theta_{N1}) \frac{\partial f}{\partial E}}{eT \int \int dE d\theta_{N1} \cos\theta_{N1} (E_F^N + E) \tau_\sigma(E, \theta_{N1}) \frac{\partial f}{\partial E}} \quad (5)$$

while the energy is shifted by Fermi energy. Now the charge and spin Seebeck coefficients are usually defined by [45],

$$S_{ch} = \frac{1}{2}(S_{up} + S_{down}) ; S_{sp} = \frac{1}{2}|S_{up} - S_{down}| \quad (6)$$

which can be computed from Eqn.(5) for $\sigma = up/down$.

The efficiency of the device depends upon a quantity called as 'Figure of Merit' (FM). To get a clear idea of the efficiency, one should compute the spin dependent FM which is given by,

$$Z_\sigma T = \frac{S_\sigma^2 G_\sigma}{K_\sigma} T \quad (7)$$

where S_σ is Seebeck coefficient, G_σ is electrical conductance, K_σ is thermal conductance, and T is absolute temperature. G_σ can be calculated from the relation $G_\sigma = \frac{dI_{NS\sigma}}{dV}$ and is given by the form,

$$G_\sigma = \frac{1}{2eR_N E_F^N} \int \int \tau_\sigma(E, \theta_{N1}) \left(-\frac{\partial f}{\partial E}\right) (E + E_F^N) dE \cos\theta_{N1} d\theta_{N1} \quad (8)$$

The thermal conductance K_σ , can be calculated from the relationship $K_\sigma = \frac{dJ_{NS\sigma}}{dT}$ where $J_{NS\sigma}$ is the thermal current flowing from the normal region to the superconducting region. In the next subsection we shall discuss how the thermal current and the thermal conductance can be calculated.

In addition, the charge FM ($Z_{ch}T$) and spin FM ($Z_{sp}T$) are defined as [45–47],

$$Z_{ch}T = \frac{S_{ch}^2 (G_{up} + G_{down}) T}{K_{up} + K_{down}} ; Z_{sp}T = \frac{S_{ch}^2 |G_{up} - G_{down}| T}{K_{up} + K_{down}} \quad (9)$$

Thermoelectric cooling. The flow of electrons can also transport the thermal energy through the junction which is responsible for the thermal current. The thermal current is defined as the rate at which the thermal energy flows from left lead to right lead. As said earlier, the left electrode, that is the normal lead serves as the cold reservoir and the right one serves as hot reservoir. The junction device is connected to an external bias voltage,

$V_B = (E_F^N - E_F^S)/e$, which drives the electrons to flow from the normal lead to the superconducting lead. Thus the electron removes the heat energy from the normal lead and transfers it to the superconducting lead which further makes the cold reservoir (normal) cool. The energy conservation allows us to write,

$$J_{NS_\sigma}(E_F^N, T^N; E_F^S, T^S) + I_{NS_\sigma}(E_F^N, T^N; E_F^S, T^S)V_B \quad (10)$$

$$= J_{SN_\sigma}(E_F^N, T^N; E_F^S, T^S)$$

The analogue between the electronic charge current and the electronic thermal current allows us to write the out-bound energy flow rate from the normal lead to the superconducting lead as,

$$J_{NS_\sigma} = \frac{1}{2e^2 R_N E_F^N} \int \int (E - eV_B)(E + E_F^N) \tau'_\sigma(E, \theta_{N1}) [f^N(E - eV_B, T^N) - f^S(E, T^S)] dE \cos \theta_{N1} d\theta_{N1} \quad (11)$$

Similarly, the reverse, that is the rate at which the superconducting lead receives the thermal energy is written as,

$$J_{SN_\sigma} = \frac{1}{2e^2 R_N E_F^N} \int \int E(E + E_F^N) \tau'_\sigma(E, \theta_{N1}) [f^N(E - eV_B, T^N) - f^S(E, T^S)] dE \cos \theta_{N1} d\theta_{N1} \quad (12)$$

while energies are shifted by Fermi energy and τ'_σ is given by the form,

$$\tau'_\sigma(E, \theta_{N1}) = 1 - |b_\sigma(E, \theta_{N1})|^2 - |a_\sigma(E, \theta_{N1})|^2 \quad (13)$$

The thermal conductance, K_σ can be calculated from $\frac{dJ_{NS_\sigma}}{dT}$. This normal-insulator-superconductor (NIS) junction can be regarded as the electronic cooling device only when $J_{NS_\sigma} > 0$, which implies that it is capable to remove the heat from the cold reservoir, thereby making it cooler.

The performance of this junction as a self-cooling device can be measured by the coefficient of the performance (COP) where COP is defined as the ratio of the heat removed from the cold reservoir to the electrical power needed for driving the system. The COP for electronic thermal current, namely, COP_σ is given by,

$$COP_\sigma = \frac{J_{NS_\sigma}}{I_{NS_\sigma} V_B} = \frac{J_{NS_\sigma}}{J_{NS_\sigma} - J_{SN_\sigma}} \quad (14)$$

Results and Discussions. – We have investigated the thermoelectric effect of a graphene based normal-insulator-superconductor (NIS) junction device in the presence of Rashba and intrinsic spin-orbit couplings assumably induced by the transition metal adatoms, where the effects of the spin-orbit couplings are mimicked by the Kane-Mele model [24]. When adatoms are adsorbed by graphene, the electrons of the outer most shell of adatoms are distributed among the carbon atoms of graphene. This causes a net positive charge in the vicinity of the adatoms and to screen this charge, electrons starts to accumulate

surrounding the adatom. This electron cloud results in an inhomogeneous electric field which cause enhanced spin-orbit couplings.

Here we include a note on the values of various parameters used for our numerical computation. To put things in perspective, we have considered some reasonable values of Δ_0 , for example, $\Delta_0 \sim (10^{-3} - 10^{-2})eV$. E_F^N has been considered as $50\Delta_0$. The Fermi velocity and the hopping parameter t_1 can be calculated from the Fermi energy through the relation $E_F = \hbar v_F k_F$ with $v_F = \frac{3t_1 a}{2\hbar}$. The strength of the NN hopping, λ_R and the NNN hopping, λ_I are varied in the range $[0 : 0.17t_1]$ and $[0 : 0.02t_1]$ respectively. In our work, the strength of the λ_R and λ_I are taken as parameters and the thermoelectric effects are computed for various choices of these parameters. Physically, it implies decorating the graphene nanoribbon by adatoms which induce the SOC couplings. It is worth mentioning that, using different techniques, such as using an external gate voltage or organic solvents etc., it is possible to enhance the SOC strengths up to a couple of orders of magnitude. Finally, the staggered term is taken as $\lambda_\nu = 0.1t_1$. The temperature difference, δT that exists across the junction is taken as, $\delta T = 0.02\Delta_0$, ensuring that the difference is indeed small.

Seebeck Coefficient and Figure of Merit. Initially we show the results for the Seebeck coefficient for a pristine graphene ($\lambda_R = \lambda_I = 0$). The variation of the Seebeck coefficient, S as function of the temperature (in units of superconducting gap, Δ_0) for a pristine graphene is shown in Fig.(2a). The Seebeck coefficient, S is dimensionless (since $e = 1$ and $k_B = 1$). To get an idea about the role of spin-orbit couplings on behaviour of the thermopower, in Fig.(2b) we present the variation of the spin resolved Seebeck coefficient, S as function of temperature for realistic values, that is, for Au decorated graphene which confirms from first principal calculations, $\lambda_I = 0.007t_1$ and $\lambda_R = 0.0165t_1$ [27]. A comparison between the two does not yield any significant change in the thermopower profile and neither one gets spin resolved signal. Thus,

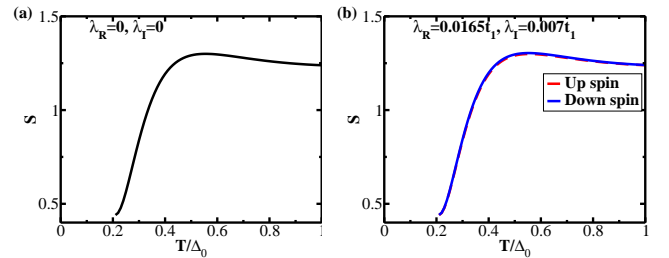


Fig. 2: (Color online) The variation of the Seebeck coefficient, S as a function of temperature, T (scaled by superconducting order parameter, Δ_0) (a) for pristine graphene, (b) for Au decorated graphene.

by some means, if we are able to enhance the SOCs by one order of magnitude compared to the values available in the Au decorated graphene, there could be noticeable

effects of SOC. Thus in Fig.(3) we have shown the thermopower profile with RSOC strengths that are larger by one order of magnitude and indeed noticeable changes are obtained with spin resolved contributions (up spin larger than that of the down spin). Thus in the latter discussions we shall use these values of the SOC's strength. In case of a normal junction (that is not a graphene based junction) in presence of the Rashba term (the intrinsic term alone should not be responsible for a noticeable spin selection), there is no spin resolved thermopower. It is clearly understood that with the inclusion of the SOC parameters, the Seebeck coefficient increases.

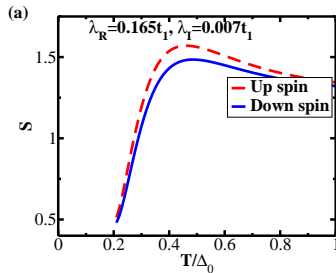


Fig. 3: (Color online) The variation of the Seebeck coefficient, S as a function of temperature, T (scaled by superconducting order parameter, Δ_0) for one order greater magnitude of RSOC parameter.

To get an idea how the spin resolved Seebeck coefficient vary with both of the spin-orbit couplings, and also to get an operating regime in the parameter space, we have shown the spin resolved Seebeck coefficient as a function of λ_R and λ_I in Fig.(4a) and Fig.(4b) with temperature, $T = 0.5\Delta_0$. The color plots yield the information of the Seebeck coefficient for different values of the RSOC and the ISOC parameters. For certain values of the RSOC parameter ($> 0.1t_1$), irrespective of the ISOC strength, both spins show higher values of thermopower. Further we have shown results for the charge and spin Seebeck coefficients in Fig.(4c) and Fig.(4d). The charge Seebeck coefficient shows higher values for larger strengths of RSOC, and for certain values of the SOC parameters, the spin Seebeck coefficient vanishes. This map aids in identifying an operating regime of the magnitude of the Seebeck coefficient corresponding to a variety of choices of λ_R and λ_I . As the strengths of SOC's correspond to presence of different adatoms, a careful choice of the periodic table may provide useful information on tunable thermopower of these junction devices.

Now we show the results on the 'Figure of Merit' (FM) which defines the efficiency of this system as a thermopower device. The variations of the spin dependent FM, $Z_\sigma T$ as the function of the spin-orbit couplings (λ_R and λ_I) are presented in Fig.(5a) and Fig.(5b). Interestingly, the down spin shows more efficiency compared to that of the up spin and hence it contradicts the behaviour of the Seebeck coefficient. Further we have shown the results for charge and spin FM in Fig.(5c) and Fig.(5d),

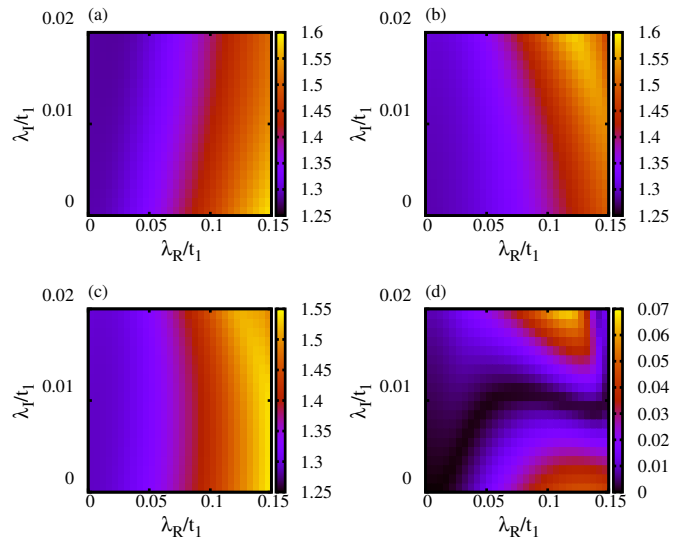


Fig. 4: (Color online) The variation of the spin resolved Seebeck coefficient, S as function of λ_R and λ_I (scaled by t_1) for (a) up spin, (b) down spin, (c) The variation of the charge Seebeck coefficient, S_{ch} as function of λ_R and λ_I (scaled by t_1), (d) The variation of the spin Seebeck coefficient, S_{sp} as function of λ_R and λ_I (scaled by t_1).

where it is observed that for higher values of ISOC the charge FM becomes larger. The spin FM becomes zero for the lower values of the RSOC parameters irrespective of the ISOC strength. Such regions, alongwith others, are shown by black patches in Fig.(5d). Thus these maps aid in deciding on the values of the parameters that may be used for maximizing the gain of these KMNIS junction devices.

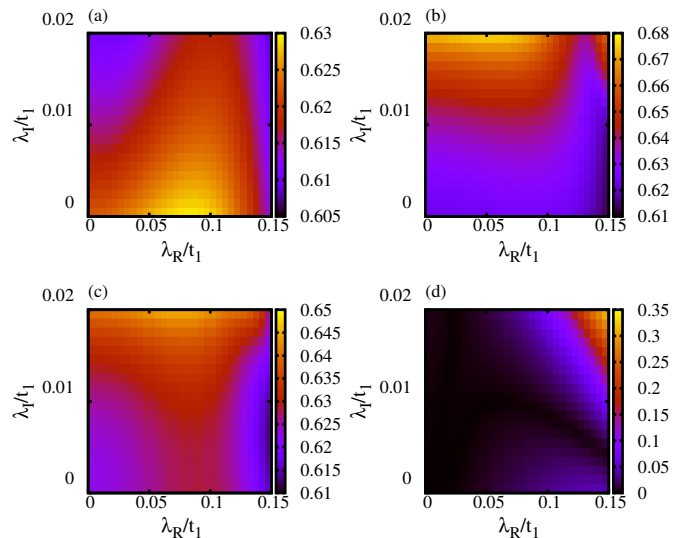


Fig. 5: (Color online) The variation of the spin resolved Figure of Merit, $Z_\sigma T$ as function of λ_R and λ_I (scaled by t_1) for (a) up spin, (b) down spin, (c) The variation of the charge FM, $Z_{ch}T$ as function of λ_R and λ_I (scaled by t_1), (d) The variation of the spin FM, $Z_{sp}T$ as function of λ_R and λ_I (scaled by t_1).

Thermoelectric cooling and coefficient of performance.

Here we show the results of the thermoelectric cooling of the KMNIS junction. To get an idea about the role of spin-orbit coupling on the thermal current, in Fig.(6a) we present the variation of a dimensionless quantity, $2J_{NS}e^2R_N/\Delta_0^2$ as a function of biasing voltage where the temperature is fixed at $T = 0.5\Delta_0$. It is evident that

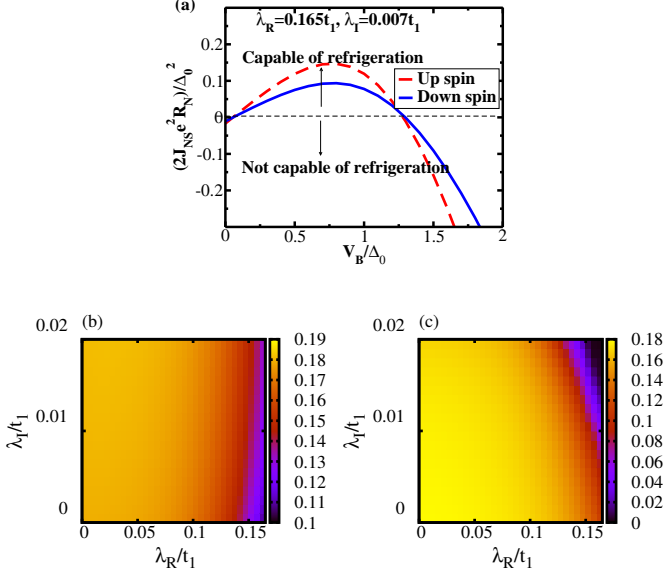


Fig. 6: (Color online) (a) The variation of the thermal current, $2J_{NS}e^2R_N/\Delta_0^2$ as a function of biasing voltage, V_B (scaled by superconducting order parameter, Δ_0). The variation of the thermal current as function of λ_R and λ_I (scaled by t_1) for (b) up spin, (c) down spin.

at zero biasing voltage, the rate of the thermal current extracted from the cold (normal) reservoir is negative. Thus, to achieve cooling effects, a lower threshold voltage of the battery, namely, V_{lower} is needed. That is, the thermoelectric cooling does not work when $V_B < V_{lower}$. Also beyond an upper threshold voltage, V_{upper} , the refrigeration effect ceases to exist. From the plots it is visible that for a very small range of the biasing voltage (having values in the vicinity of the superconducting order parameter), the thermoelectric cooling process is efficient and the maximum refrigeration occurs at around, $V_B \sim 0.9\Delta_0$. Moreover, we have checked that a lower threshold of the voltage, V_{lower} required to trigger the cooling effect does not depend on the choice of the SOC parameters.

Next we have shown spin resolved thermal current as the function of both the spin-orbit couplings in Fig.(6b) and Fig.(6c) which provides an idea of the desired (for maximum thermoelectric cooling) range of values of the RSOC, the ISOC parameters and the corresponding thermal current. The biasing voltage is fixed at $V_B = 0.5\Delta_0$. For higher values of the RSOC parameter, the thermoelectric cooling for both spins becomes smaller. As the SOC parameters are tunable, the color plots give useful information on the tunable thermoelectric cooling.

Here we show the results of the performance of the KMNIS junction as a self-cooling device. To recapitulate, a measure of the performance and the efficiency of the KMNIS junction as a thermoelectric nano-refrigerator is defined by the coefficient of performance (COP). Fig.(7)

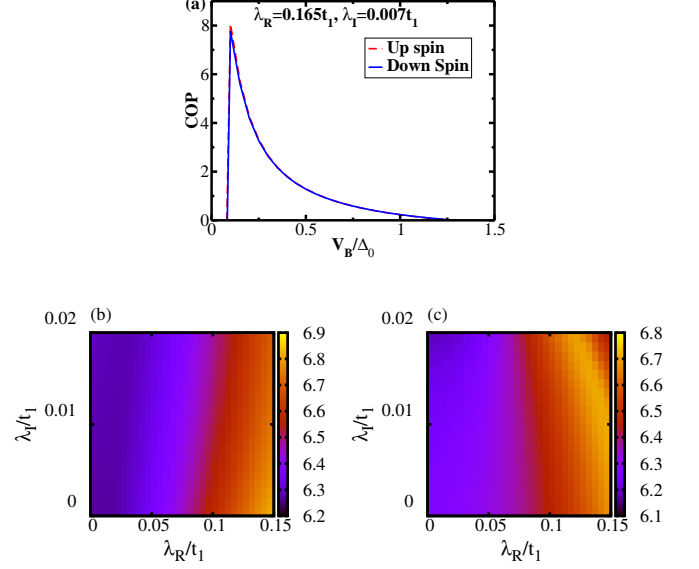


Fig. 7: (Color online) (a) The variation of the coefficient of performance, COP as a function of biasing voltage, V_B (scaled by superconducting order parameter, Δ_0). The variation of COP as function of λ_R and λ_I (scaled by t_1) for (b) up spin, (c) down spin.

reveals that for a narrow range of the biasing voltage, the nano refrigeration works (namely, $\sim 0.06\Delta_0 - \Delta_0$). Since Δ_0 is in meV range for conventional superconductor, the operating voltage is low. Further it is understood that when the driving voltage exceeds the value of the superconducting order parameter, Δ_0 , the refrigeration vanishes, irrespective of the strengths of SOC.

Finally to complete our enumeration of the tunability of a KMNIS junction, the COP is plotted as a function of the RSOC and ISOC strengths in Fig.(7b) and Fig.(7c). The color plots provide the idea of the range of values of the RSOC, the ISOC and the corresponding coefficient of performance. The biasing voltage is fixed at $V_B = 0.125\Delta_0$ where the COP shows large value. It is clear that the RSOC helps to enhance the COP for both spins. The color plots provide a helpful hint on the tunable coefficient of performance.

Conclusion. – In summary, we have investigated the thermoelectric properties of a KMNIS junction in presence of spin-orbit couplings by employing BTK theory in great details. We have investigated the Seebeck coefficient and the thermoelectric Figure of Merit of this junction device and explained how SOC play a role in determining these properties. Further the thermoelectric cooling of this junction device and its performance as a cooling device have been studied in details. It is clear that the thermoelec-

tric properties are sensitive to the SOC parameters. As the strength of the SOC terms can be manipulated via different adatoms or using gate voltages etc, we may infer that it is possible to achieve a precision tuning of the thermoelectric properties of these junction devices.

REFERENCES

- [1] K. S. Novoselov, A. K. Geim, S. V. Morozov, D. Jiang, M. I. Katsnelson, I. V. Grigorieva, S. V. Dubonos, and A. A. Firsov, *Nature* **438**, 197 (2005)
- [2] A. De Martino, L. Dell'Anna, and R. Egger, *Phys. Rev. Lett.* **98**, 066802 (2007).
- [3] A. H. C. Neto, F. Guinea, N. M. R. Peres, K. S. Novoselov, and A. K. Geim, *Rev. Mod. Phys.* **81**, 109 (2009)
- [4] F. Bonaccorso, Z. Sun, T. Hasan, and A. C. Ferrari, *Nat. Photonics* **4**, 611 (2010)
- [5] P. Avouris, *Nano. Lett.* **10**, 4285 (2010)
- [6] A. G. Moghaddam and M. Zareyan, *Phys. Rev. Lett.* **105**, 146803 (2010)
- [7] D. Pesin and A. H. MacDonald, *Nat. Mat.* **11**, 409 (2012)
- [8] W. Han, R. K. Kawakami, M. Gmitra, and J. Fabian, *Nat. Nanotechnol.* **9**, 794 (2014)
- [9] B. Ghosh, *J. Appl. Phys.* **109**, 013706 (2011)
- [10] Y. Zhang, Y. W. Tan, H. L. Stormer, and P. Kim, *Nature* **438**, 201 (2005)
- [11] K. S. Novoselov, Z. Jiang, Y. Zhang, S. V. Morozov, H. L. Stormer, U. Zeitler, J. C. Maan, G. S. Boebinger, P. Kim, and A. K. Geim, *Science* **315**, 1379 (2007)
- [12] M. I. Katsnelson, K. S. Novoselov, and A. K. Geim, *Nat. Phys.* **2**, 620 (2006)
- [13] C. W. J. Beenakker, *Rev. Mod. Phys.* **80**, 1337 (2008)
- [14] M. Zareyan, H. Mohammadpour, and A. G. Moghaddam, *Phys. Rev. B* **78**, 193406 (2008)
- [15] B. Uchoa and A. H. C. Neto, *Phys. Rev. Lett.* **98**, 146801 (2007)
- [16] A. I. Buzdin, *Rev. Mod. Phys.* **77**, 935 (2005)
- [17] H. B. Heersche, P. Jarillo-Herrero, J. B. Oostinga, L. M. Vandersypen, and A. F. Morpurgo, *Solid state Comm.* **143**, 72 (2007)
- [18] A. A. Balandin, S. Ghosh, W. Bao, I. Calizo, D. Teweldebrhan, F. Miao, and C. N. Lau, *Nano Lett.* **8**, 902 (2008)
- [19] Y. M. Zuev, W. Chang, and P. Kim, *Phys. Rev. Lett.* **102**, 096807 (2009)
- [20] D. Dragoman and M. Dragoman, *Appl. Phys. Lett.* **91**, 203116 (2007)
- [21] K. Uchida, S. Takahashi, K. Harii, J. Ieda, W. Koshibae, K. Ando, S. Maekawa, and E. Saitoh, *Nature* **455**, 778 (2008)
- [22] C. M. Jaworski, R. C. Myers, E. Johnston-Halperin, and J. P. Heremans, *Nature* **487**, 210 (2012)
- [23] P. Wei, W. Bao, Y. Pu, C. N. Lau, and J. Shi, *Phys. Rev. Lett.* **102**, 166808 (2009)
- [24] C. L. Kane and E. J. Mele, *Phys. Rev. Lett.* **95**, 226801 (2005)
- [25] H. Min, J. E. Hill, N. A. Sinitsyn, B. R. Sahu, L. Kleinman, and A. H. MacDonald, *Phys. Rev. B* **74**, 165310 (2006)
- [26] Y. G. Yao, F. Ye, X.-L. Qi, S.-C. Zhang, and Z. Fang, *Phys. Rev. B* **75**, 041401 (2007)
- [27] C. Weeks, J. Hu, J. Alicea, M. Franz, and R. Wu, *Phys. Rev. X* **1**, 021001 (2011)
- [28] L. Kou, B. Yan, F. Hu, S.-C. Wu, T. O. Wehling, C. Felser, C. Chen, and T. Frauenheim, *Nano. Lett.* **13**, 6251 (2013)
- [29] J. Zhang, C. Triola, and E. Rossi, *Phys. Rev. Lett.* **112**, 096802 (2014)
- [30] K. Zollner, T. Frank, S. Irmer, M. Gmitra, D. Kochan, and J. Fabian, *Phys. Rev. B* **93**, 045423 (2015)
- [31] D. Marchenko, A. Varykhalov, M. R. Scholz, G. Bihlmayer, E. I. Rashba, A. Rybkin, A. M. Shikin, and O. Rader, *Nat. Commun.* **3**, 1232 (2012)
- [32] Y. S. Dedkov, M. Fonin, U. Rudiger and C. Laubschat, *Phys. Rev. Lett.* **100**, (2008) 107602
- [33] F. Calleja, H. Ochoa, M. Garnica, S. Barja, J. J. Navarro, A. Black, M. M. Otrokov, E. V. Chulkov, A. Arnau, A. L. V. de Parga, F. Guinea, and R. Miranda, *Nat. Phys.* **11**, 43 (2015)
- [34] J. Mastomaki, S. Roddaro, M. Rocci, V. Zannier, D. Ercolani, L. Sorba, I. J. Maasilta, N. Ligato, A. Fornieri, E. Strambini, and F. Giazotto, *Nano Research* **10**, 3468 (2017)
- [35] Y. S. Liu, B. C. Hsu, and Y. C. Chen, *J. Phys. Chem.* **115**, 6111 (2011)
- [36] M. Nahum, T. M. Eiles, and J. M. Martinis, *Appl. Phys. Lett.* **65**, 3123 (1994)
- [37] A Bardas and D Averin, **52**, 17(1995)
- [38] M. Wysokinski, *Acta Physica Polonica A*, **122**, 163905 (2012)
- [39] M. Wysokinski and J Spalek, *J. Appl. Phys.* **113**, 163905 (2013)
- [40] A. V. Feshchenko, J. V. Koski, and J. P. Pekola, *Phys. Rev. B* **90**, 201407 (R) (2014)
- [41] A. M. Clark, A. Williams, S. T. Ruggiero, M. L. Berg, and J. N. Ullom, *Appl. Phys. Lett.* **84**, 625 (2004)
- [42] N. A. Miller, G. C. O'Neil, J. A. Beall, G. C. Hilton, K. D. Irwin, D. R. Schmidt, L. R. Vale, and J. N. Ullom, *Appl. Phys. Lett.* **92**, 163501 (2008)
- [43] P. Kapri and S. Basu, *Euro. Phys. Lett.*, **124**, 17002, (2018)
- [44] K. R. Patton and M. R. Geller, *Phys. Rev. B* **64**, 155320 (2001)
- [45] R. Swirkowicz, M. Wierzbicki, J. Barana, *Phys. Rev. B* **80**, 195409 (2009)
- [46] M. Hatami, G.E.W. Bauer, Q.F. Zhang, P.J. Kelly, *Phys. Rev. B* **79**, 174426 (2009)
- [47] X.B. Chen, Y.Z. Liu, B.L. Gu, W.H. Duan, F. Liu, *Phys. Rev. B* **90**, 121403 (2014)
- [48] C. L. Kane and E. J. Mele, *Phys. Rev. Lett.* **95**, 146802 (2005).
- [49] C W J Beenakker, *Phys. Rev. Lett.* **97**, 067007 (2006).